Applied Surface Science 425 (2017) 553–557

Contents lists available at ScienceDirect

Applied Surface Science

journal homepage: www.elsevier.com/locate/apsusc

Full length article

Fabrication of large-area high-aspect-ratio periodic nanostructures on various substrates by soft X-ray interference lithography

Chaofan Xue[a,1], Jun Zhao[a,1], Yanqing Wu[a,*], Huaina Yu[a], Shumin Yang[a], Liansheng Wang[a], Wencong Zhao[a], Qiang Wu[b], Zhichao Zhu[b], Bo Liu[b], Xia Zhang[c], Wenchao Zhou[d], Renzhong Tai[a,*]

[a] Shanghai Institute of Applied Physics, Chinese Academy of Sciences, Shanghai Synchrotron Radiation Facility, Shanghai, 201800, PR China
[b] Shanghai Key Laboratory of Special Artificial Microstructure Materials and Technology, School of Physics Science and Engineering, Tongji University, Shanghai, 200092, PR China
[c] Shandong Provincial Key Laboratory of Laser Polarization and Information Technology, Qufu Normal University, Qufu, 273165, China
[d] State Key Laboratory of Applied Optics, Changchun Institute of Optics, Fine Mechanies and Physics, Chinese Academy of Sciences, Changchun, 130033, PR China

ARTICLE INFO

Article history:
Received 1 June 2017
Received in revised form 26 June 2017
Accepted 3 July 2017
Available online 8 July 2017

Keywords:
Synchrotron radiation
Soft X-ray interference lithography
Large-area high-aspect-ratio nano periodic arrays
Photonic crystals

ABSTRACT

Periodic nanostructures have attracted considerable interest and been applied in many fields. However, nanostructures of sufficiently large areas and depths are necessary for the development of practical devices. In this study, large-area high-aspect-ratio periodic nanostructures were fabricated by using a hybrid technology based on X-ray interference lithography, and then the patterns were transferred onto various substrates successfully. The final periodic nanostructures on the substrate attained measurements up to square centimetres with depths greater than 200 nm.

1. Introduction

With the rapid development of nano-processing technology, nanostructures have attracted considerable interest due to their widespread applications in many fields, including catalysis [1–4], sensing [5–8], data storage [9], optoelectronics [10] and fields related to biology [11]. Furthermore, certain performances of nanostructures can be drastically improved if the nanostructures are arranged in an ordered array. It is expected that high performance devices will be developed on the basis of periodic nanostructures, and therefore, the fabrication of larger-area periodic nanostructures will be quite important for the development of these devices. Focused ion beam etching and electron beam lithography are two direct writing methods. High-resolution nanostructures can be obtained by using these methods although there is a high preparation cost in both time and capital that must be due to the large-area nanostructures because of the nature of the serial writing process. Methods based on self-assembled templates can be applied to the fabrication of large-area nanostructures at a low cost with high throughput and high efficiency. However, the area that can be obtained with perfect periodicity is limited to within several tens of micrometres [12,13] because long-range ordered structures are difficult to prepare using this method. The interference lithography method is a powerful way to produce highly ordered structures because of the strict periodicity of the interference pattern. Due to the diffraction limit, a traditional visible laser is not suitable for fabricating nanostructures. Thanks to the rapid development of synchrotron facilities, extreme ultraviolet (EUV) and soft X-rays produced by an undulator have been adopted as novel sources in interference lithography because of the high brilliance and good coherence of these rays [14–20]. A single-exposure patterned area is about several $10^2 \times 10^2\ \mu m^2$, which is mainly dictated by the mask area in multi-beam X-ray interference lithography (XIL). Unfortunately, this area is also too small to fabricate a practical device. Recently, a novel large-area XIL stitching technique was developed at the XIL beamline at the Shanghai Synchrotron Radiation Facility (SSRF) [21]. The patterned area can be

* Corresponding authors.
E-mail addresses: wuyanqing@sinap.ac.cn (Y. Wu), tairenzhong@sinap.ac.cn (R. Tai).
[1] These authors contributed equally to this work.

http://dx.doi.org/10.1016/j.apsusc.2017.07.010
0169-4332/

readily stitched together to up to several square centimetres and even larger with this technique, and the development of a practical device is possible based on such a large area.

Similar to other lithography methods, the exposure patterns are first recorded on the photoresist in the XIL, and then the patterns are transferred onto the substrate. A variety of substrates can be used in the XIL because for the substrates, there are no special requirements such as electrical conductivity. Structures with sufficient depth have contributed to the expansion of the processing window in post-treatment. A wider processing window is important for preparing the sample successfully. In addition, high-aspect-ratio patterns are a physical requirement in some research fields. For example, scintillators are critical in radiation detection systems. The detection efficiency of such systems is improved if photonic crystals (PhCs) are introduced onto the surface of the scintillator, and the high-aspect-ratio periodic structures of these PhCs can contribute to the extraction of more photons. To obtain structures of sufficient depth, a novel soft X-ray interference lithography (SXIL) technique was developed at the XIL beamline at SSRF [22]. In this technique, a photon energy of 140 eV instead of the traditional 92.5 eV was selected to increase the transmission rate in the photoresist while maintaining a good beamline optical efficiency. Compared with the pattern obtained by applying 92.5 eV photons, when the photon energy is changed to 140 eV, the depth can be increased from less than 100 up to 300 nm.

Large-area XIL stitching technique and SXIL are two new developed nano-processing technologies based on XIL at SSRF. These two novel technologies have been developed independently and realized large exposure area and high-aspect-ratio periodic nanostructures, respectively. In this study, large-area high-aspect-ratio periodic nanostructures were prepared on various substrates successfully by combining the two new technologies. The experimental results show that these two technologies can be combined perfectly and the hybrid technology shows a powerful ability to prepare large-area high-aspect-ratio periodic nanostructures.

2. Experimental

The XIL exposure experiments were carried out at the XIL beamline [23], which is a branch of the BL08U1A [24] beamline at SSRF. An APPLE-II type undulator is used to produce high brilliant photons, which decide the relative spectral width of the radiation spectra is about 1/42. In the experiments, 140-eV coherent photons were optimized and delivered by the beamline and then irradiated onto a homemade grating mask. The total size of the grating mask is about $1 \times 1\ mm^2$, so the spot size is optimized to be $1.5 \times 1.5\ mm^2$ by comprehensive considering uniformity, coherence and photon flux. The coherence can be controlled by adjusting the aperture and the exit slit in our beamline. In this case the coherent length was estimated to be 2 mm at the mask plane by the mutual optical intensity (MOI) model [25]. The coherent photon flux density is measured to be about 1.8×10^{15} phs/s/cm^2 by a calibrated photodiode (AXUV100G, IRD). Multi-beams for interference were obtained using the grating mask. If the period of the mask grating was p, the exposed pattern period of the first diffraction needed to be p/2 for two-beam interference, $p/\sqrt{3}$ for three-beam interference and $p/\sqrt{2}$ for four-beam interference. Fig. 1 shows the schematic diagram of the fabrication process of the periodic nanostructures on a silicon substrate. PMMA (MicroChem PMMA A4, 950 k) was spin-coated on a double-side polished silicon wafer to obtain a 300-nm-thick PMMA layer. Prebaking was required at 180 °C for 1.5 min. The photoresist was then exposed by the interference beam generated by the mask grating. By moving the silicon wafer step by step, the exposure areas could be stitched together area by area. After XIL exposure, the PMMA was developed in MIBK diluted at 1:3 in IPA for 45 s, rinsed with alcohol for 30 s and finally dried with a gentle N_2 flow.

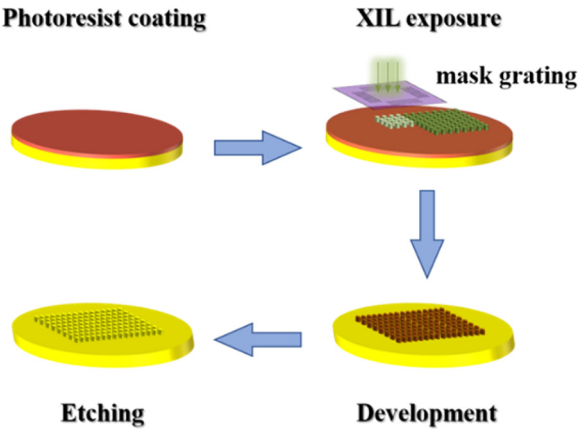

Fig. 1. Schematic diagram of the fabrication process for large-area high-aspect-ratio periodic nanostructures.

3. Results and discussion

Although the larger area exposure technology and the SXIL technology were developed independently, these two technologies are not mutually exclusive and can be naturally integrated. In this case, 140-eV photons are used instead of 92.5 eV photons in the SXIL while higher photon energy is also very favourable for the larger exposure area. To stitch the exposure area together area by area, an order-sorting aperture (OSA) is necessary to block the zero-order diffraction from the mask grating. Meanwhile, the ±first-order diffraction from the mask grating must not be blocked by the OSA, otherwise the pattern at the edge region will be different from that at the centre area. Therefore, the tolerance for the moving distance δ for the OSA is highly constrained along the beam direction. The δ can be estimated as follows:

$$\delta \approx \frac{d(L-D)}{2\lambda}$$

where L is the distance between two gratings, D is the width of the grating, d is the grating period and λ is the wavelength of the incident beam. The distance δ greatly depends on the grating period d and usually it is about several hundred microns. In consideration of the thickness of the OSA (usually about 300–400 μm), the OSA has to be very close to the wafer. Higher photon energy implies a smaller diffraction angle according to the grating equation when the grating period is the same, which will lead to a longer tolerance for the moving distance of the OSA as shown in Fig. 2. When 140 eV photons are used instead of 92.5 eV photons, the δ_{140eV} will be about 1.5 times longer than the $\delta_{92.5eV}$.

The final exposure result is shown in Fig. 3, where a 280 nm period four-grating mask is applied. Ultimately, the total pattern area reached $1.2 \times 1.2\ cm^2$ with a period of 200 nm. Thanks to the top-up operation mode at SSRF, the photon flux that arrived at the photoresist could be kept stable for a long time. Therefore, the pattern area was mainly dictated by the travel range of the motor and could be up to several square centimetres or even more. To verify the photoresist depth after XIL exposure, the wafer was sectioned and observed through a scanning electron microscope (SEM). The cross-sectional SEM image reveals that the depth of the nanostructure was about 300 nm with an aspect ratio of up to 3.

However, the photoresist pattern cannot be applied directly in most cases, so the pattern transfer is important and requires further research. One of the advantages of XIL is that there is no special requirement for the substrate, thus periodic nanostructures can be

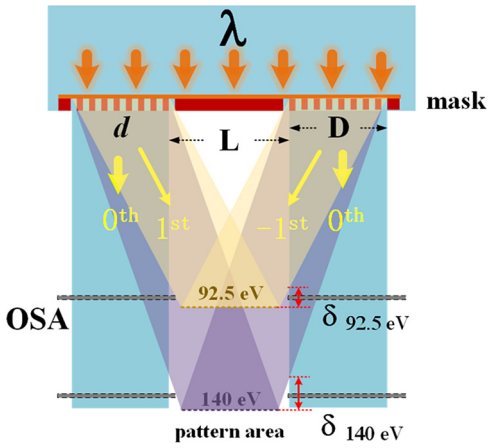

Fig. 2. Moving distance tolerance of the OSA in large-area XIL exposure with different photon energies.

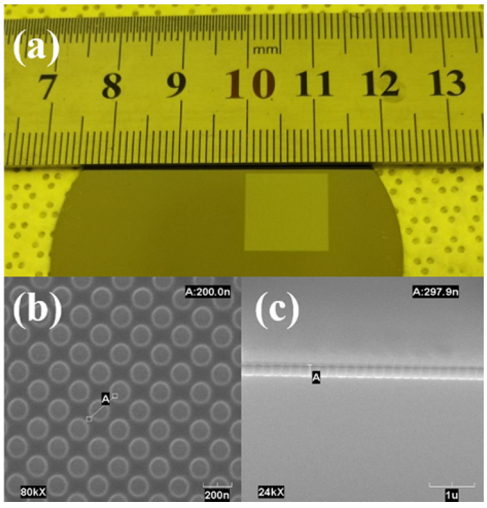

Fig. 3. Exposure result: (a) the total exposure area is $1.2 \times 1.2\,cm^2$, (b) the period of the nanostructure is 200 nm and (c) the depth of the nanostructure is about 300 nm.

fabricated and transferred onto different substrates. Up to now, this hybrid technology has been open to the users of the XIL beamline. One of the important applications in this domain is fabricating PhCs on scintillators. Scintillators are critical in radiation detection system applications, such as medical imaging, high-energy physics experiments and homeland security [26]. The detection efficiency of such systems would be improved if PhCs were introduced onto the surface of the scintillator because the periodic structures of the PhCs would contribute to the extraction of more photons. As proven in our previous work, the high-aspect-ratio periodic structures of PhCs can contribute to the extraction of more photons [22]. To develop a practical device on the basis of the excellent performance of PhCs, larger area periodic nanostructures have been fabricated on the surface of quartz and different scintillators such as $Y_3Al_5O_{12}$:Ce (YAG:Ce), $Bi_4Ge_3O_{12}$ (BGO), which have no electrical conductivity. Fig. 4 shows the result of a large-area exposure pattern fabricated on a quartz substrate by using an 840 nm period mask grating. Fig. 4(b) shows the atomic force microscope (AFM) image of the photoresist pattern. The duty cycle of the pattern was designed to be greater than 1 for the subsequent atomic layer deposition (ALD). The structure depth was about 300 nm as shown in Fig. 4(c), which is consistent with the SEM result on the silicon wafer shown in Fig. 3(c).

Fig. 5 shows large-area nanostructures that have been transferred onto a YAG:Ce crystal successfully by using an inductively coupled plasma (ICP) etch system (Plasmalab ICP 180, Oxford Instruments, Bristol, UK). The total pattern area in the YAG:Ce crystal was about $0.8 \times 0.8\,cm^2$ as shown in Fig. 5(a). Such a large area can meet the practical requirements of certain devices. Fig. 5(b) shows the AFM images of the nanostructures in the YAG:Ce crystal. Because of the strict periodicity of the interference field, the nanostructures fabricated by XIL showed good consistent orientation of the periodicity, which is also an advantage of the interference lithography method. Furthermore, the orientations kept constant in all the exposure areas. The AFM line-scan profile shown in Fig. 5(c) indicates that the depth of the nanostructures on the YAG:Ce crystal is about 220 nm, which illustrates that the depth of the unetched photoresist structure is at least 220 nm where the etch selectivity ratio is nearly 1. PMMA A4 photoresist was selected to obtain a thick coating layer. And this further determines the depth of the nanostructures in the photoresist. Combining the properties of the photoresist and the transmission rate of the X-ray in this energy range, a 300-nm deep photoresist structure can be consistently obtained. This implies that the high-aspect-ratio of the nanostructures is mainly decided by the period. Though the high-aspect-ratio is less than 1 in this study, it was determined by the 600-nm pattern period, which is optimized for maximum light extraction efficiency. This ratio for the pattern can be up to 3 if the pattern period goes down to 200 nm [22].

According to various applications, different processes can be chosen for pattern transfer. Compared with the etching process, the lift-off process has a narrower processing window, which requires higher quality photoresist patterns. The height of the final nanostructures is variable depending on the materials in the lift-off processing. Consider gold as an example: the height of the Au nanostructure is usually less than 1/3 of the photoresist thickness. Therefore, a high-aspect-ratio photoresist pattern will provide a wider processing window for the lift-off process. The sample shown in Fig. 6(a) was prepared for magneto-optical effect research. A 5×5 array which consists of 25 $2 \times 2\,mm^2$ areas was prepared on a 3-inch-diameter $Si/Au/SiO_2$ substrate. After the lithography

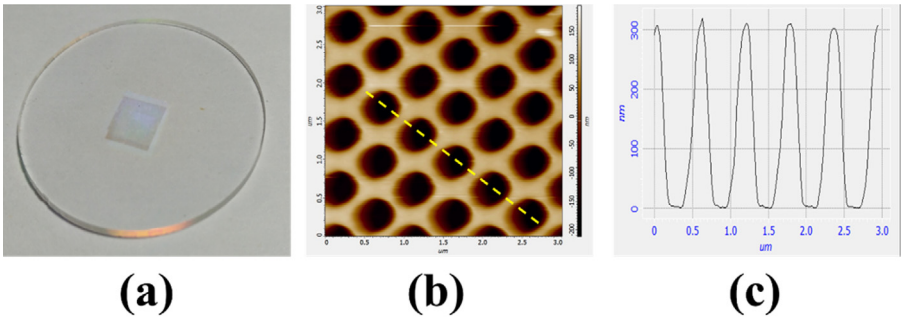

Fig. 4. (a) Periodic nanoholes prepared on quartz with a total area of $0.6 \times 0.6\,cm^2$, (b) AFM imaging of the periodic nanoholes and (c) the height curve of the prepared periodic nanoholes, which is consistent with the SEM result on the silicon wafer.

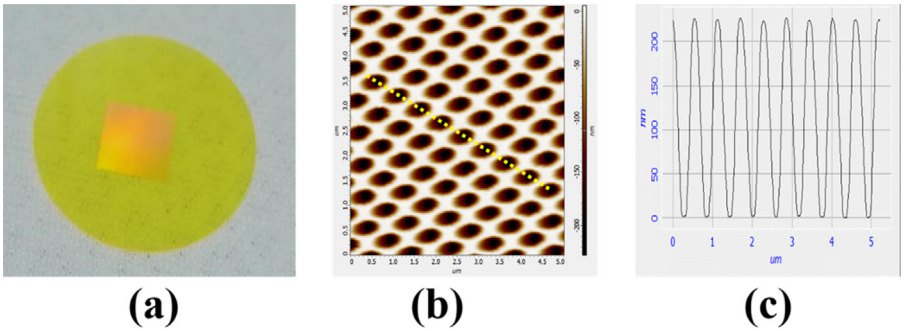

Fig. 5. (a) Periodic nanoholes prepared on the YAG:Ce screen with a total area of $0.8 \times 0.8\,cm^2$, (b) AFM imaging of the periodic nanoholes and (c) the height curve of the prepared periodic nanoholes.

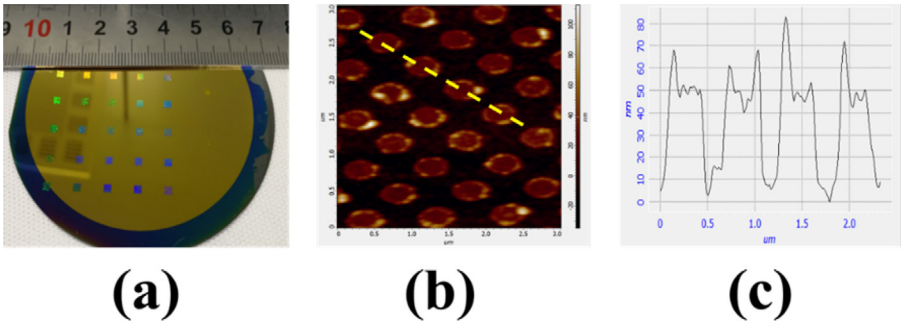

Fig. 6. (a) Periodic Au nanocylinders prepared on a Si/Au/SiO_2 substrate by e-beam evaporation, (b) AFM imaging of the periodic Au nanocylinders and (c) the height curve of the prepared periodic Au nanocylinders.

was completed, a Cr (5 nm)/Au (50 nm) layer was evaporated by an e-beam evaporation system (QPrep Deposition System, MANTIS, Oxfordshire, UK) in a 1×10^{-8} mbar vacuum environment, where chromium was used as an adhesive layer to prevent the gold from falling off. After evaporation, the resist layer was lifted off in acetone at room temperature in an ultrasonic bath for 10 min. AFM imaging of the obtained periodic Au nanocylinders is shown in Fig. 6(b), and the height curve of the Au nanocylinders is shown in Fig. 6(c). As expected, the Au nanocylinders with a height of about 50 nm were transferred successfully onto the SiO_2 substrate. In our in-house study, the height of the Au nanocylinders attained 70 nm by lift-off processing when the thickness of the photoresist was 300 nm. Thus, 50 nm Au cylinders can be fabricated and provided to users consistently.

4. Conclusions

Periodic nanostructures have attracted considerable interest and can be applied in many areas. However, most of the research remains in the laboratory stage and has not been developed into a practical device because nanostructures with sufficiently large areas and depths are difficult to fabricate efficiently and inexpensively. In this study, periodic nanostructures with an area up to square centimetres were fabricated by using a hybrid technology based on XIL technology. The photoresist patterns were fabricated with a depth about 300 nm and transferred onto different substrates successfully with a depth of over 200 nm by etching and over 50 nm by lift-off processing. Up to now, this hybrid technology has been open to users of the XIL beamline.

Acknowledgements

The authors wish to thank the staff of the BL08U beamline at SSRF. This work was supported by the Youth Innovation Promotion Association (No. 2017306), The National Key Research and Development Program of China (No. 2016YFA0401302), the National Natural Science Foundation of China (Grant Nos. 11205236, 11275255 and 11475251), the Open Research Project of Large Scientific Facility from the Chinese Academy of Sciences: Study on Self-Assembly Technology and Nanometer Arrays with Ultra-High Density and the State Key Laboratory of applied optics.

References

[1] Y.M. Li, G.A. Somorjai, Nanoscale advances in catalysis and energy applications, Nano Lett. 10 (7) (2010) 2289–2295.
[2] M.A. Mahmoud, F. Saira, M.A. El-Sayed, Experimental evidence for the nanocage effect in catalysis with hollow nanoparticles, Nano Lett. 10 (9) (2010) 3764–3769.
[3] J. Zeng, Q. Zhang, J. Y.Chen, Y.N. Xia, A comparison study of the catalytic properties of Au-based nanocages, nanoboxes, and nanoparticles, Nano Lett. 10 (1) (2010) 30–35.
[4] A.S.K. Hashmi, Homogeneous gold catalysis beyond assumptions and proposals—characterized intermediates, Angew. Chem. Int. Ed. 49 (2010) 5232–5241.
[5] H. Ko, S. Singamaneni, V.V. Tsukruk, Nanostructured surfaces and assemblies as SERS media, Small 4 (10) (2008) 1576–1599.
[6] R.A. Tripp, R.A. Dluhy, Y.P. Zhao, Novel nanostructures for SERS biosensing, Nano Today 3 (3–4) (2008) 31–37.
[7] W.E. Smith, Practical understanding and use of surface enhanced Raman scattering/surface enhanced resonance Raman scattering in chemical and biological analysis, Chem. Soc. Rev. 37 (2008) 955–964.
[8] M.E. Stewart, C.R. Anderton, L.B. Thompson, J. Maria, S.K. Gray, J.A. Rogers, R.G. Nuzzo, Nanostructured plasmonic sensors, Chem. Rev. 108 (2) (2008) 494–521.
[9] A.J. Hong, C.C. Liu, Y. Wang, J. Kim, F.X. Xiu, S.X. Ji, J. Zou, P.F. Nealey, K.L. Wang, Metal nanodot memory by self-assembled block copolymer lift-off, Nano Lett. 10 (1) (2010) 224–229.
[10] S. Conoci, S. Petralia, P. Samori, F.M. Raymo, S.D. Bella, S. Sortino, Optically transparent, ultrathin Pt films as versatile metal substrates for molecular optoelectronics, Adv. Funct. Mater. 16 (11) (2006) 1425–1432.
[11] D.A. Giljohann, D.S. Seferos, W.L. Daniel, M.D. Massich, P.C. Patel, C.A. Mirkin, Gold nanoparticles for biology and medicine, Angew Chem. Int. Ed. 49 (19) (2010) 3280–3294.
[12] Z.C. Zhu, B. Liu, C.W. Cheng, H. Chen, M. Gu, Y. Yi, R. Mao, Broadband light output enhancement for scintillator using whispering-gallery modes in nanospheres, Phys. Status Solidi (a) 211 (7) (2014) 1583–1588.

[13] Z.C. Zhu, B. Liu, C.W. Cheng, Y. Yi, H. Chen, M. Gu, Improved light extraction efficiency of cerium-doped lutetium-yttrium oxyorthosilicate scintillator by monolayers of periodic arrays of polystyrene spheres, Appl. Phys. Lett. 102 (2013) 071909.
[14] D. Fan, Y. Ekinci, Photolithography reaches 6 nm half-pitch using extreme ultraviolet light, J. Micro/Nanolithography MEMS MOEMS 15 (3) (2016) 033505.
[15] W. Karim, S.A. Tschupp, M. Oezaslan, T.J. Schmidt, J. Gobrecht, J.A. Bokhoven, Y. Ekinci, High-resolution and large-area nanoparticle arrays using EUV interference lithography, Nanoscale 7 (2015) 7386–7393.
[16] N. Mojarad, J. Gobrecht, Y. Ekinci, Beyond EUV lithography: a comparative study of efficient photoresists' performance, Sci. Rep. 5 (2015) 9235.
[17] N. Mojarad, J. Gobrecht, Y. Ekinci, Interference lithography at EUV and soft X-ray wavelengths: principles, methods, and applications, Microelectron. Eng. 143 (2015) 55–63.
[18] N. Mojarad, M. Hojeij, L. Wang, J. Gobrecht, Y. Ekinci, Single-digit-resolution nanopatterning with extreme ultraviolet light for the 2.5 nm technology node and beyond, Nanoscale 7 (2015) 4031.
[19] N. Mojarad, D. Fan, J. Gobrecht, Y. Ekinci, Broadband interference lithography at extreme ultraviolet and soft x-ray wavelengths, Optics Lett. 39 (8) (2014) 2286–2289.
[20] V. Auzelyte, H.H. Solak, Y. Ekinci, R. MacKenzie, J. Voros, S. Olliges, R. Spolenak, Large area arrays of metal nanowires, Microelectron. Eng. 85 (2008) 1131–1134.
[21] C.F. Xue, Y.Q. Wu, F.Y. Zhu, S.M. Yang, H.G. Liu, J. Zhao, L.S. Wang, R.Z. Tai, Development of broadband X-ray interference lithography large area exposure system, Rev. Sci. Instrum. 87 (2016) 043303.
[22] J. Zhao, Y.Q. Wu, C.F. Xue, S.M. Yang, L.S. Wang, F.Y. Zhu, Z.C. Zhu, B. Liu, Y. Wang, R.Z. Tai, Fabrication of high aspect ratio nanoscale periodic structures by the soft X-ray interference lithography, Microelectron. Eng. 170 (2017) 49–53.
[23] S.M. Yang, L.S. Wang, J. Zhao, C.F. Xue, H.G. Liu, Z.J. Xu, Y.Q. Wu, R.Z. Tai, Developments at SSRF in soft X-ray interference lithography, Nucl. Sci. Tech. 26 (2015) 010101.
[24] C.F. Xue, Y. Wang, Z. Guo, Y.Q. Wu, X.J. Zhen, M. Chen, J.H. Chen, S. Xue, Z.Q. Peng, Q.P. Lu, R.Z. Tai, High-performance soft x-ray spectromicroscopy beamline at SSRF, Rev. Sci. Instrum. 81 (2010) 103502.
[25] X.Y. Meng, C.F. Xue, H.N. Yu, Y. Wang, Y.Q. Wu, R.Z. Tai, Numerical analysis of partially coherent radiation at soft x-ray beamline, Opt. Express 23 (23) (2015) 29675–29686.
[26] M. Nikl, A. Yoshikawa, Recent R&D trends in inorganic single-crystal scintillator materials for radiation detection, Adv. Opt. Mater. 3 (2015) 463–481.